Enhancing electrocatalytic CO_2 reduction using a system-integrated approach to catalyst discovery

Thomas Burdyny*[,1] and Wilson A. Smith*[,1]

[1]Materials for Energy Conversion and Storage, Department of Chemical Engineering, Delft University of Technology, 2629 HZ Delft, The Netherlands

[*] Correspondence and requests for materials can be addressed to Thomas Burdyny (t.e.burdyny@tudelft.nl) and Wilson A. Smith (W.smith@tudelft.nl)

Modelling CO_2 concentrations and pH in aqueous electrolytes

The models used to create the CO_2 and pH profiles in Fig. 3 are based upon previously presented works by these authors as well as others. The equations describing carbonate equilibrium were presented by Gupta et al.[1] and have been previously used to describe the concentration profiles of active CO_2 reduction species in both H-cell[2–4] and gas-diffusion layer configurations.[5,6] The equations and assumptions used in the model are presented here for completeness.

A catalyst capable of reducing CO_2 to value-added products such as CO, CH_4, C_2H_4, etc. in an electrochemical cell requires a source of CO_2, protons (H^+) and electrons. Electrons can be provided via a counter-reaction at the anode, typically the oxygen-evolution reaction, while protons are provided directly by the electrolyte in various forms. The final reagent, CO_2, must be provided externally to the cell and is present at the catalyst as dissolved CO_2. The saturated concentration of dissolved CO_2 in the electrolyte is a function temperature and pressure according to Henry's law and a function of salt concentration and type in the electrolyte, which can be calculated using Sechenov's equation.[7]

Modelling of the CO_2 reduction reaction in an H-cell configuration

In an H-cell configuration, dissolved CO_2 is provided from the bulk electrolyte where gaseous CO_2 is bubbled into the aqueous solution and dispersed throughout the catholyte container using agitation or flow in a channel (Fig. 2a). It is generally assumed in experimentation that the bulk electrolyte is saturated with CO_2 at all times. As CO_2 is consumed at the cathode, it is replenished from the bulk electrolyte. Due to fluid boundary layers, however, this replenishment is limited by diffusive processes, causing the concentration of CO_2 to be lower than that of the bulk concentration. The maximum CO_2 reduction currents that can be maintained are directly proportional to the thickness of the diffusive region and the type and

concentration of electrolyte being used. Here in this model, the diffusion region is assumed to be a constant 50 μm, as described in the main text and shown illustrated in Fig. 2b.

The diffusive region is then modelled between x = 0 μm and x = 50 μm using the following equations taking into account the bicarbonate-carbonate equilibrium reactions:

$$\frac{\partial [CO_2]}{\partial t} = D_{CO_2} \frac{\partial^2 [CO_2]}{\partial x^2} - [CO_2][OH^-]k_{1f} + [HCO_3^-]k_{1r} \tag{S1}$$

$$\frac{\partial [HCO_3^-]}{\partial t} = D_{HCO_3^-} \frac{\partial^2 [HCO_3^-]}{\partial x^2} + [CO_2][OH^-]k_{1f} - [HCO_3^-]k_{1r} - [HCO_3^-][OH^-]k_{2f} + [CO_3^{2-}]k_{2r} \tag{S2}$$

$$\frac{\partial [CO_3^{2-}]}{\partial t} = D_{CO_3^{2-}} \frac{\partial^2 [CO_3^{2-}]}{\partial x^2} + [HCO_3^-][OH^-]k_{2f} - [CO_3^{2-}]k_{2r} \tag{S3}$$

$$\frac{\partial [OH^-]}{\partial t} = D_{OH^-} \frac{\partial^2 [OH^-]}{\partial x^2} - [CO_2][OH^-]k_{1f} + [HCO_3^-]k_{1r} - [HCO_3^-][OH^-]k_{2f} + [CO_3^{2-}]k_{2r} \tag{S4}$$

At the left-hand boundary (x = 0 μm), CO_2 is consumed and OH⁻ is generated according to the fluxes described by Eqs. S5 and S6, while at x = 50 μm each species (CO_2, HCO_3^-, CO_3^{2-}, OH⁻) is prescribed as its bulk equilibrium value:

$$\frac{\dot{n}_{CO2}}{A} = \frac{-j}{F}\left(\frac{FE_{CO}}{n_{e,CO}}\right) \quad , @ \; x = 0 \tag{S5}$$

$$\frac{\dot{n}_{OH^-}}{A} = \frac{j}{F} \quad , @ \; x = 0 \tag{S6}$$

where j is the prescribed geometric current density, F is Faraday's constant, FE_{CO} is the Faradaic efficiency of CO production assumed to be 90% in all cases and $n_{e,CO}$ is the number of electrons required per CO molecule, equal to 2.

Modelling of the CO_2 reduction reaction in a gas-diffusion layer configuration

In a gas-diffusion layer configuration, CO_2 can be supplied from a high concentration gaseous source of CO_2 in close proximity to the reduction catalyst, typically using a hydrophobic-hydrophilic substrate to form a gas-liquid interface within nm's of the catalyst layer Fig. e. The diffusion pathway of dissolved CO_2 to the catalyst layer is then substantially smaller than in an H-cell, despite still dissolving into the electrolyte prior to reacting at the catalyst's surface. Here we assume the catalyst layer has a porosity of 60% and is 100 nm thick. As

most catalysts are hydrophilic, we assume that the start of the catalyst is present immediately adjacent to the hydrophobic-hydrophilic gas-liquid interface (x = 0). To reach the centre of the catalyst layer, CO_2 must then diffuse on the order of 50 nm. Any formed gas products are observed experimentally to diffuse back into the gas-phase and thus gas evolution is not observed in the catholyte chamber, which reduces liquid mass transport versus the H-cell scenario.[8] Additionally, the use of flow-channels on the order of $1 - 10$ mm in height will reduce the Reynold's number of the fluid flow as compared to a openly-stirred H-cell. For these reasons the liquid diffusion thickness is assumed to be 200 µm in Fig. 2c and d instead of the 50 µm in the H-cell case. This impacts the diffusion of generated hydroxide as well as the concentrations of the buffering media (HCO_3^- and CO_3^{2-}). Further diffusion thickness variations are provided in Fig. S1 and produce the same conclusion regarding the >12 pH at the electrode at >200 mA/cm^2 current densities for all electrolytes.

The diffusion-reaction equations are similar to the H-cell scenario with the addition of source and sink terms for CO_2 and OH^- within the porous catalyst layer according to Eqs. S11 and S12.

$$\frac{\partial [CO_2]}{\partial t} = D_{CO_2} \frac{\partial^2 [CO_2]}{\partial x^2} - [CO_2][OH^-]k_{1f} + [HCO_3^-]k_{1r} + R_{CO2} \tag{S7}$$

$$\frac{\partial [HCO_3^-]}{\partial t} = D_{HCO_3^-} \frac{\partial^2 [HCO_3^-]}{\partial x^2} + [CO_2][OH^-]k_{1f} - [HCO_3^-]k_{1r} - [HCO_3^-][OH^-]k_{2f} + [CO_3^{2-}]k_{2r} \tag{S8}$$

$$\frac{\partial [CO_3^{2-}]}{\partial t} = D_{CO_3^{2-}} \frac{\partial^2 [CO_3^{2-}]}{\partial x^2} + [HCO_3^-][OH^-]k_{2f} - [CO_3^{2-}]k_{2r} \tag{S9}$$

$$\frac{\partial [OH^-]}{\partial t} = D_{OH^-} \frac{\partial^2 [OH^-]}{\partial x^2} - [CO_2][OH^-]k_{1f} + [HCO_3^-]k_{1r} - [HCO_3^-][OH^-]k_{2f} + [CO_3^{2-}]k_{2r} + R_{OH} \tag{S10}$$

$$R_{CO2} = \begin{cases} \frac{-j}{F}\left(\frac{FE_{CO}}{n_{e,CO}}\right)\frac{\varepsilon}{L_{catalyst}} & , \; 0 \leq x \leq L_{catalyst} \\ 0 & , \quad x > L_{catalyst} \end{cases} \tag{S11}$$

$$R_{OH} = \begin{cases} \frac{j}{F}\frac{\varepsilon}{L_{catalyst}} & , \; 0 \leq x \leq L_{catalyst} \\ 0 & , x > L_{catalyst} \end{cases} \tag{S12}$$

The reaction is assumed to occur homogeneously throughout the thickness of the catalyst layer, $L_{catalyst}$, here assumed as 100 nm.
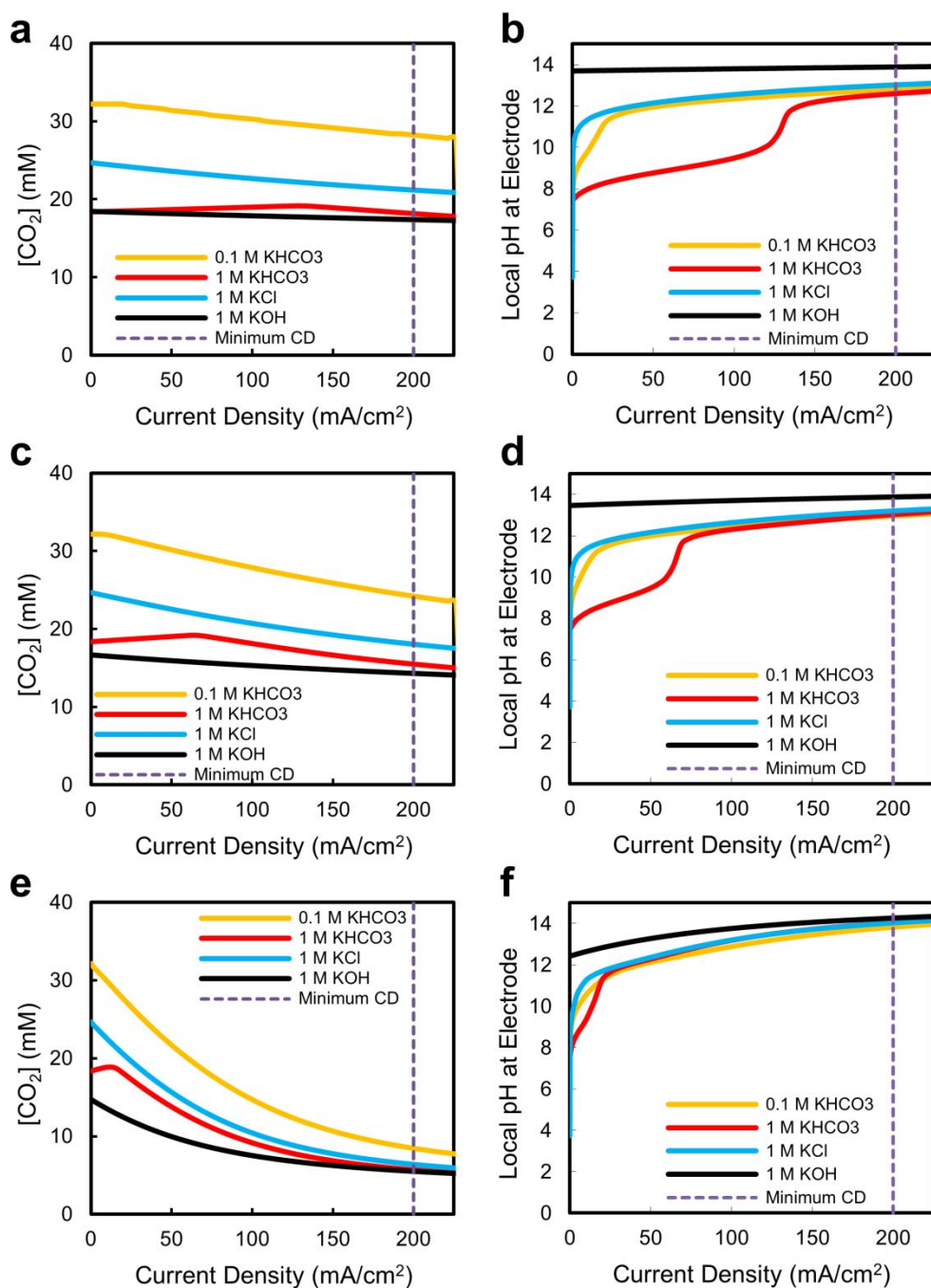
Fig. S1: Predicted CO_2 concentration and pH within the catalyst layer of a gas-diffusion electrode assuming a liquid boundary layer thickness of 50 µm (a,b), 100 µm (c,d) and 200 µm (e,f). All simulated curves assume a CO_2 reduction Faradaic efficiency of 90% through a two-electron transfer process with 10% H_2 evolution as well as a 100 nm thick porous catalyst layer.
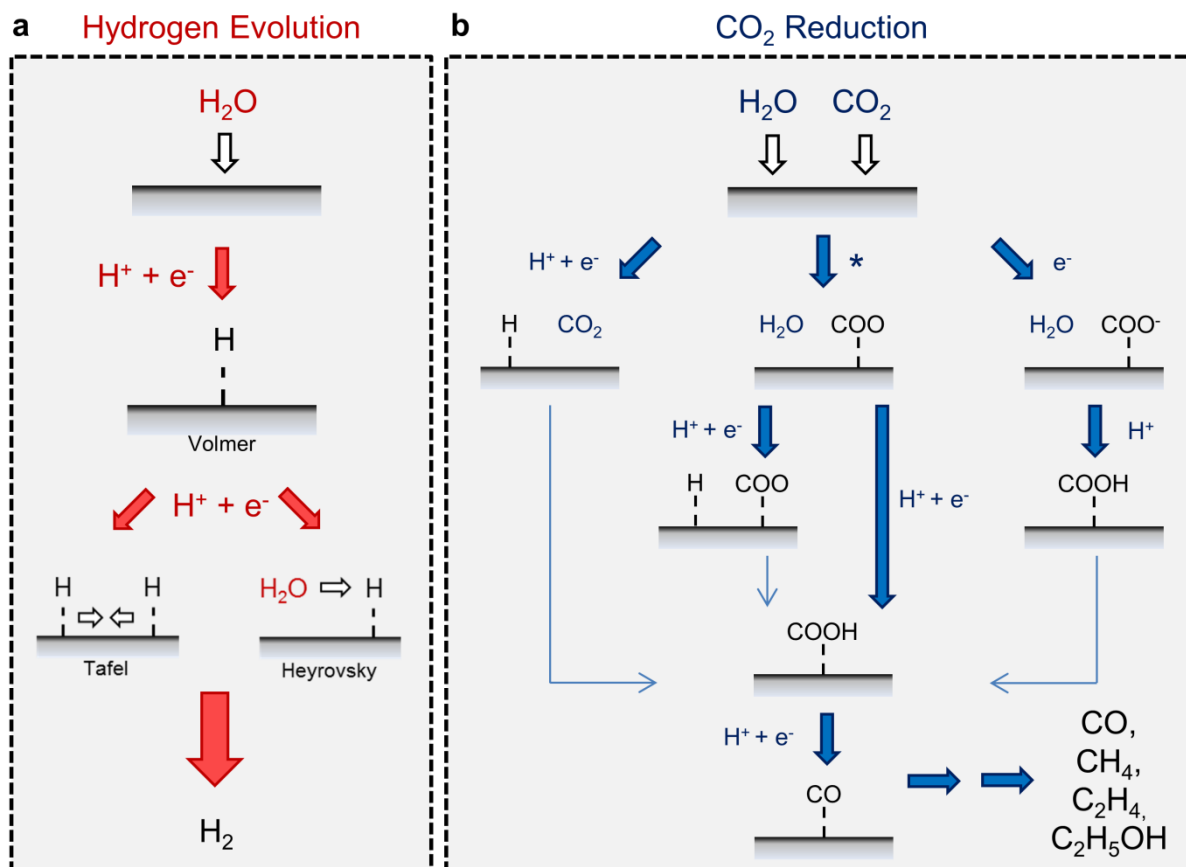
Fig. S2: (a) The general reaction pathway for the Hydrogen Evolution Reaction (HER) in neutral and basic media; HER is the primary competing reaction to CO_2 reduction. (b) Possible reaction pathways for electrochemical CO_2 reduction to adsorbed CO (*CO) showing variations of the initial proton-electron transfer step that may be thermodynamically or kinetically affected by changes in the local reaction environment.
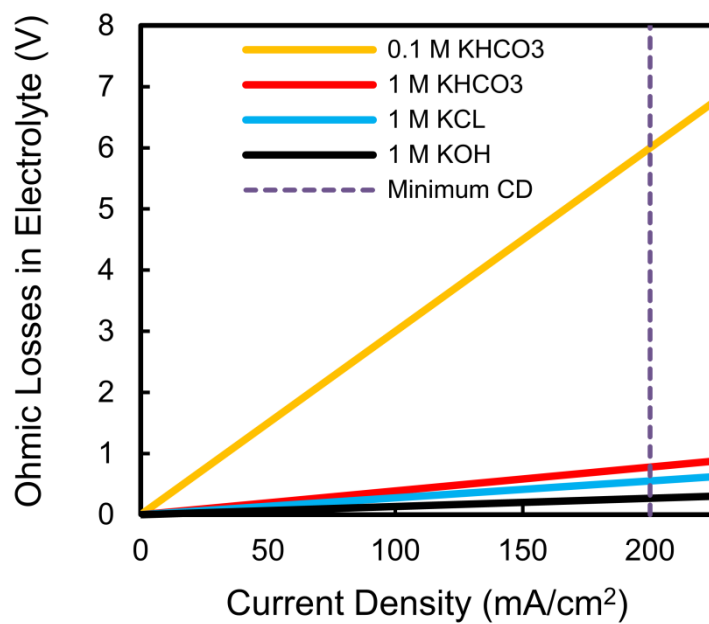
Fig. S3: Expected ohmic losses as a function of current density for commonly-used electrolytes in an electrochemical cell with a combined 3 mm catholyte and anolyte thickness. The y-axis has been extended versus Fig. 4 to show the full ohmic losses of the 0.1 M $KHCO_3$ electrolyte at 200 mA/cm^2.

References

1. Gupta, N., Gattrell, M. & MacDougall, B. Calculation for the cathode surface concentrations in the electrochemical reduction of CO_2 in $KHCO_3$ solutions. *J. Appl. Electrochem.* **36,** 161–172 (2006).

2. Burdyny, T. *et al.* Nanomorphology-Enhanced Gas-Evolution Intensifies CO2 Reduction Electrochemistry. *ACS Sustain. Chem. Eng.* **5,** 4031–4040 (2017).

3. Pang, Y. *et al.* Joint tuning of nanostructured Cu-oxide morphology and local electrolyte programs high-rate CO2 reduction to C2H4. *Green Chem.* **19,** 4023–4030 (2017).

4. Singh, M. R., Clark, E. L. & Bell, A. T. Effects of electrolyte, catalyst, and membrane composition and operating conditions on the performance of solar-driven electrochemical reduction of carbon dioxide. *Phys. Chem. Chem. Phys.* **17,** 18924–18936 (2015).

5. seifitokaldani, ali *et al.* Hydronium-Induced Switching Between CO2 Electroreduction Pathways. *J. Am. Chem. Soc.* (2018). doi:10.1021/jacs.7b13542

6. Dinh, C.-T. *et al.* CO2 electroreduction to ethylene via hydroxide-mediated copper catalysis at an abrupt interface. *Science* **360,** 783–787 (2018).

7. Weisenberger S. & Schumpe A. Estimation of gas solubilities in salt solutions at temperatures from 273 K to 363 K. *AIChE J.* **42,** 298–300 (2004).

8. Sequeira, C. a. C., Santos, D. M. F., Šljukić, B. & Amaral, L. Physics of Electrolytic Gas Evolution. *Braz. J. Phys.* **43,** 199–208 (2013).